ACS OMEGA

http://pubs.acs.org/journal/acsodf

Article

Spontaneous Coassembly of the Protein Terthiophene into Fluorescent Electroactive Microfibers in 2D and 3D Cell Cultures

Ilaria Elena Palamà,*[,§] Gabriele Maiorano,[§] Francesca Di Maria, Mattia Zangoli, Andrea Candini, Alberto Zanelli, Stefania D'Amone, Eduardo Fabiano, Giuseppe Gigli, and Giovanna Barbarella

Cite This: *ACS Omega* 2022, 7, 12624−12636

Read Online

ACCESS | Metrics & More | Article Recommendations | Supporting Information

ABSTRACT: Protein-based microfibers are biomaterials of paramount importance in materials science, nanotechnology, and medicine. Here we describe the spontaneous in situ formation and secretion of nanostructured protein microfibers in 2D and 3D cell cultures of 3T3 fibroblasts and B104 neuroblastoma cells upon treatment with a micromolar solution of either unmodified terthiophene or terthiophene modified by mono-oxygenation (thiophene → thiophene *S*-oxide) or dioxygenation (thiophene → thiophene *S*,*S*-dioxide) of the inner ring. We demonstrate via metabolic cytotoxicity tests that modification to the *S*-oxide leads to a severe drop in cell viability. By contrast, unmodified terthiophene and the respective *S*,*S*-dioxide cause no harm to the cells and lead to the formation and secretion of fluorescent and electroactive protein−fluorophore coassembled microfibers with a large aspect ratio, a micrometer-sized length and width, and a nanometer-sized thickness, as monitored in real-time by laser scanning confocal microscopy (LSCM). With respect to the microfibers formed by unmodified terthiophene, those formed by the *S*,*S*-dioxide display markedly red-shifted fluorescence and an increased *n*-type character of the material, as shown by macroscopic Kelvin probe in agreement with cyclovoltammetry data. Electrophoretic analyses and Q-TOF mass spectrometry of the isolated microfibers indicate that in all cases the prevalent proteins present are vimentin and histone H4, thus revealing the capability of these fluorophores to selectively coassemble with these proteins. Finally, DFT calculations help to illuminate the fluorophore−fluorophore intermolecular interactions contributing to the formation of the microfibers.

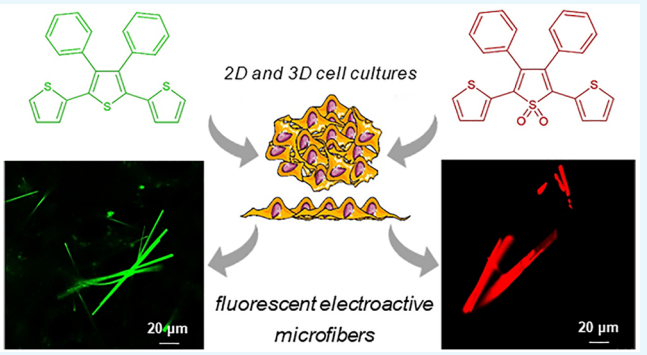

INTRODUCTION

The self-assembly of proteins into nanostructured microfibers is a growing research area that has attracted great attention in the last years and been the subject of numerous in vitro studies.[1] One of the main objectives of these investigations is to elucidate the nucleation and growth mechanisms and dynamics of natural protein aggregates, generally through the computational design and synthesis of specific peptides capable of self-assembling into nano- or microfibers via hydrogen bonding, $\pi-\pi$ stacking, hydrophobic or hydrophilic interactiosns, or other types of nonbonding intermolecular interactions. Several studies of protein self-assembly in a cellular environment, concerning a variety of objectives, have also been reported,[2,3] and several factors promoting fiber formation, such as pH, enzymes, ligand−receptor interactions, or auxiliary factors generated through sophisticated synthetic biology methods, have been described.[2] This particular attention to the formation of protein fibrils is related to their importance in the onset and development of some severe neurodegenerative disorders such as Alzheimer's disease.[4] On the other hand, these spontaneously assembled micrometer-sized fibers have great potential as biomaterials for medical and technological applications. In this frame, it has been shown that small hydrophobic natural or synthetic molecules play an important role in the formation of nanostructured protein microfibers as driving factors for aggregation. Indeed, they may act as mediators for the interaction between two protofibrils and favor the lateral growth of micrometer-sized fibers.[5−7] For example, hierarchical assembly into microfibers with the assistance of curcumin has been demonstrated in the cases of collagen[7] and other engineered proteins.[5] It has been found that the concentration of curcumin is directly related to increased protein aggregation but does not alter the secondary structure, thus imparting greater thermal stability to the system. In our studies, we have employed biocompatible and

Received: November 25, 2021
Accepted: February 25, 2022
Published: April 6, 2022

https://doi.org/10.1021/acsomega.1c06677
ACS Omega 2022, 7, 12624−12636

membrane-permeable fluorescent and semiconductor thiophene-based molecules to promote the in situ assembly of proteins into microfibers in live cells and small living organisms.[8,9] We have reported that upon the spontaneous uptake of a physiological solution of fluorescent 2,6-diphenyl-3,5-dimethyl-dithieno[3,2-b:2′,3′-*d*]thiophene-4,4-dioxide (DTTO), live mouse embryonic fibroblasts (3T3) secrete nanostructured green fluorescent microfibers mainly made of type I collagen that display a helical supramolecular organization.[8] The fluorophore, which accumulates in the perinuclear region where the intracellular proteins are formed, is recognized by the protein and progressively incorporated via metabolic pathways during the phase of protocollagen formation, leading to spontaneously coassembled supramolecular protein−fluorophore microfibers.

The collagen−fluorophore microfibers are then extruded into the extracellular matrix from which they can be isolated and analyzed. We have also shown that, thanks to the semiconducting properties of the fluorophore and its supramolecular arrangement, the microfibers are electroactive in addition to fluorescent. Thus, the fluorophore transfers additional properties, namely fluorescence and electroactivity, to the targeted protein. Using the same approach, the treatment of live B104 neuroblastoma cells, which do not produce collagen, with DTTO leads to the formation of green fluorescent microfibers mainly made of vimentin.[10] When both fiber types, namely type I collagen/DTTO and vimentin/DTTO, were used as substrates for cell cultures, it was found that the different protein compositions of these biomaterials induce very different cellular behavior, from the shredding of the microfibers, and subsequent nontoxic internalization, to cell death. More recently, we have demonstrated that DTTO is incorporated by freshwater polyp *Hydra vulgaris* with no signs of toxicity, forming green fluorescence-conductive protein−DTTO microfibers that have a prevalently coiled-coil conformation and a significant contribution from the β-sheet secondary structure.[9]

Owing to their properties and interaction modalities with intracellular proteins, the thiophenes are able to promote the secretion of fluorescent microfibers that are peculiarly different from already known small-molecule fluorophores. Unfortunately, since the relationship between molecular structure, membrane permeability, and nonbonding interactions with intracellular proteins remains elusive, the number of such thiophenes is very limited.[8−11] So far, we have been able to identify new entries only by means of a patient trial-and-error search of appropriate molecular structures that are at the same time membrane-permeable, nontoxic, fluorescent, and chemically and optically stable. Nevertheless, this search is worth the trouble, since expanding the tool box of the thiophens of this type would allow the development of a new, particularly simple, and noninvasive technique—entirely based on the ability of the fluorophore to interact with specific proteins through nonbonding interactions—to label and track intracellular proteins in the complex cell environment and also confer them additional properties.

In the present study, we report on a structurally correlated set of fluorescent terthiophenes (Scheme 1) investigated for the formation of microfibers in live cells. The object of the study is to treat 3T3 fibroblasts and neuroblastoma B104 cells in 2D systems (monolayers on flat surfaces) or grown as spheroids (cells allowed to grow in three dimensions) with micromolar solutions of the unmodified terthiophene **1** or the

Scheme 1. Structures of Unmodified Terthiophene (1) and Terthiophene Modified by Mono-Oxygenation (2) or Dioxygenation (3) of the Inner Ring

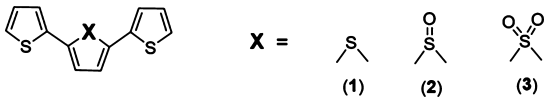

oxygenated terthiophenes **2** and **3** in order to assess the effect of sulfur functionalization on the formation of microfibers and their functional properties. It is known that in oligo and polythiophenes the functionalization of thiophene sulfur with oxygen has a profound impact on the optoelectronic properties of the system.[11] In particular, the functionalization to *S*,*S*-dioxide changes the electronic properties of a semiconducting oligothiophene from *p*-type (a material with a larger hole concentration than electron concentration) to *n*-type (a material with a larger electron concentration than hole concentration).[12] Thus, the question arises whether the changes in the optical and electronic properties of the terthiophene administered to the cells affect the properties of the microfibers formed in a predictable manner. We find that sulfur functionalization of the inner ring with one single oxygen causes cell death, whereas functionalization with two oxygens causes no harm to the cells and induces the predicted changes in the functional properties of the microfibers.[11] In particular, functionalization to the *S*,*S*-dioxide causes a shift of the Fermi energy level toward the vacuum, a signature of the reversal of prevalent charge carriers from holes (*p*-type semiconducting material) to electrons (*n*-type semiconducting material), in agreement with cyclovoltammetry data and Kelvin probe experiments. In this respect it is worth noting that a similar change was already reported and discussed for thiophene-based microfibers deposited on glass.[11] Owing to the fluorescence properties of **1** and **3**, the formation of the microfibers inside the cells can be followed in real-time by laser scanning confocal microscopy (LSCM). Once separated from the cells, the microfibers are analyzed by electrophoretic techniques, Q-TOF mass spectrometry, atomic force microscopy (AFM), and a macroscopic Kelvin probe. Finally, with the aid of DFT calculations, the charge distribution and aggregation properties of terthiophenes **1**−**3** were investigated, helping to illuminate the origin of the observed behaviors.

RESULTS AND DISCUSSION

The molecular structures and the synthesis of compounds **1**−**3** are shown in Scheme 2. The synthesis was carried out considering that fluorophores for application in live cells have to be prepared with the degree of highest purity (for experimental details, see the Synthesis section in the SI). Thus, technologies such as ultrasound for the preparation of the brominated intermediates **1a**−**3a** and microwaves for the cross-coupling reaction of thiophene bromides with thiophene stannanes were employed.[11,13] Use of ultrasound and microwaves ensured high reaction rates, chemoselectivity, and the presence of very few easily separated by products.

Figure 1A shows the normalized absorption and photoluminescence spectra of **1**−**3** together with the corresponding cyclovoltammograms and the HOMO−LUMO energy diagram. As expected,[10,13] the absorption wavelengths increase upon thiophene oxygenation in parallel with photoluminescence wavelengths, which go from green (**1**) to orange (**2**) and red (**3**). The voltammograms of **1**−**3** and the corresponding

https://doi.org/10.1021/acsomega.1c06677
ACS Omega 2022, 7, 12624−12636

Scheme 2. Synthetic Pattern for the Preparation of 1−3[a]

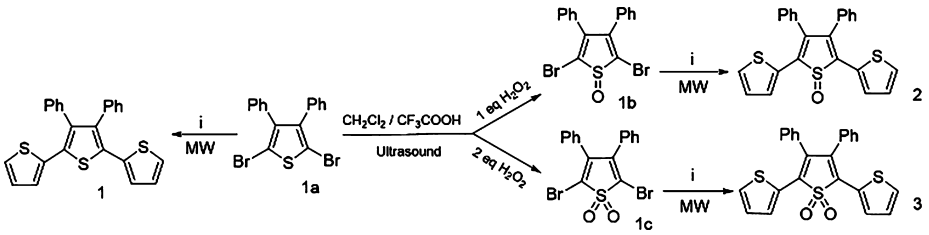

[a]Reagents and conditions are as follows: (i) 2-thienylthiophene, [1,1′-bis(diphenylphosphino)ferrocene]dichloropalladium(II), Na_2CO_3 and THF/H_2O (2:1) at 80 °C for 25 min. MW = microwave.

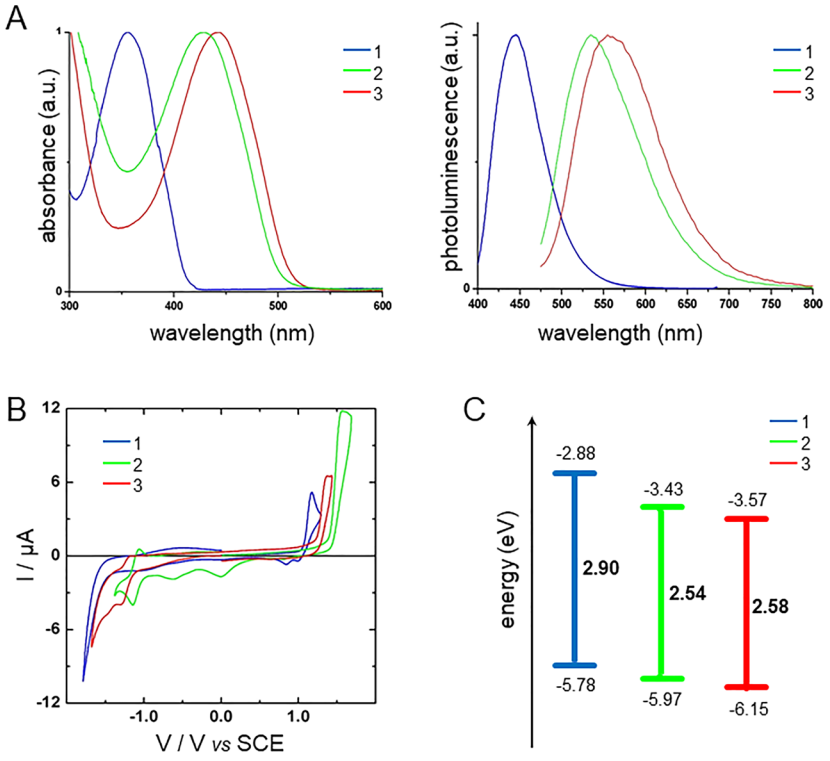

Figure 1. (A) Normalized absorption and photoluminescence spectra of compounds **1−3** in CH_2Cl_2. The excitation wavelength is at the maximum absorption. (B) Cyclic voltammograms recorded in 0.2 mmol L^{-1} $(C_4H_9)_4NClO_4$ in CH_2Cl_2 and (C) HOMO−LUMO energy diagram of compounds **1−3**.

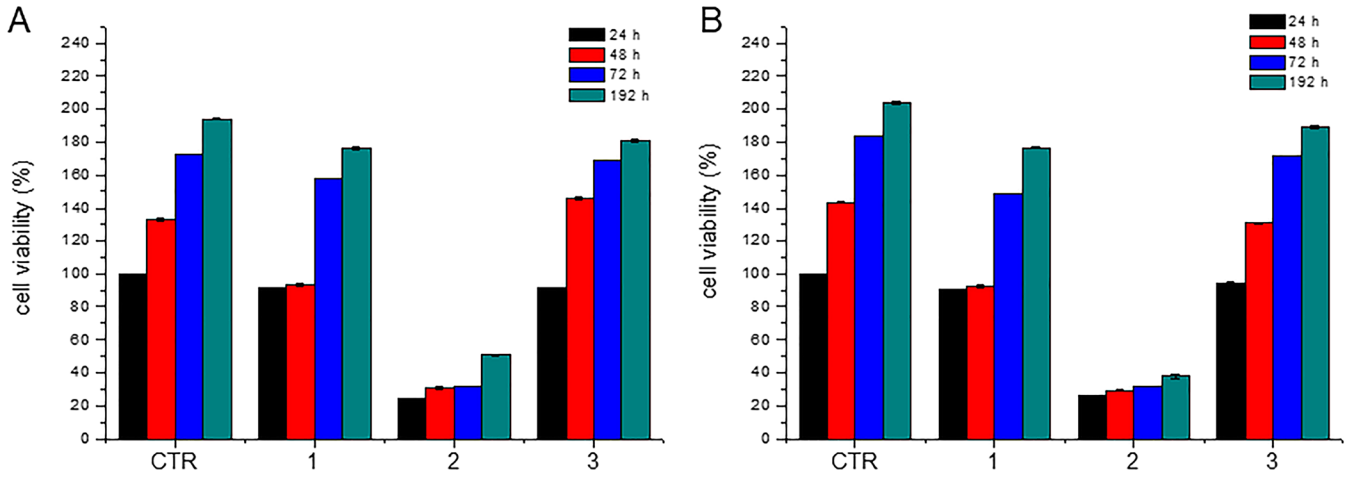

Figure 2. MTT cytotoxicity tests on (A) 3T3 and (B) B104 cells treated with compounds **1−3** compared to untreated cells (CTR). Representative measurements were taken from three distinct sets of data, and no significant difference between values at different time points was observed at $P < 0.05$ with Student's *t*-test.

https://doi.org/10.1021/acsomega.1c06677
ACS Omega 2022, 7, 12624−12636

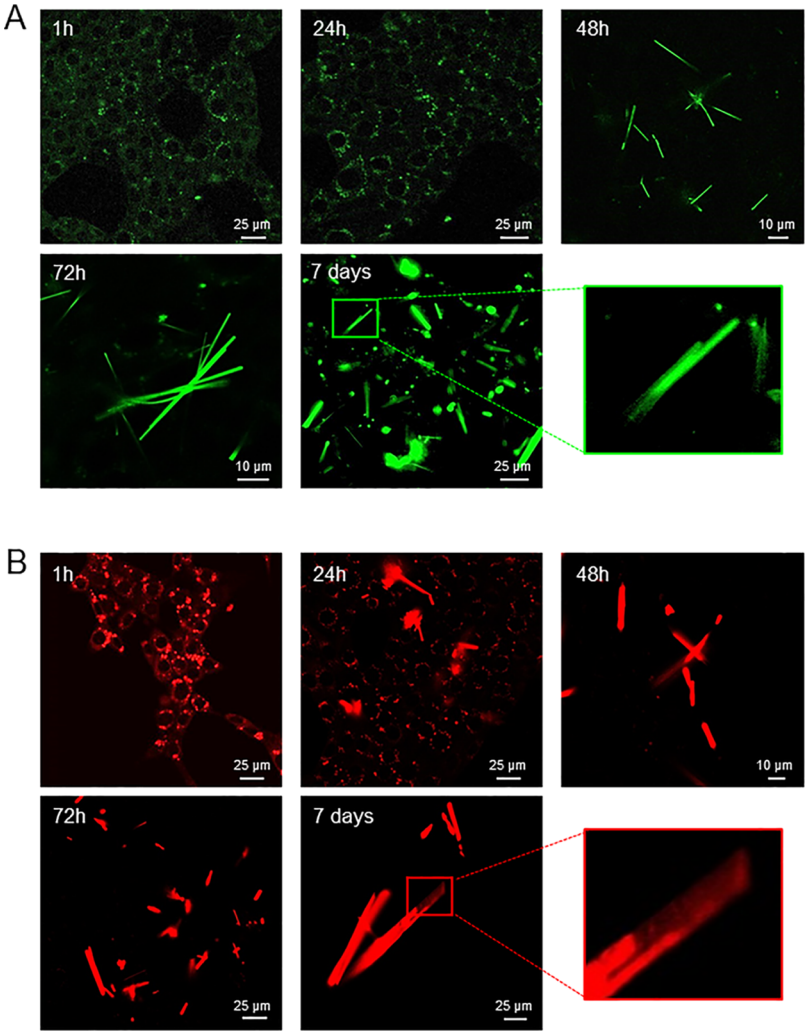

Figure 3. LSCM images of live 3T3 fibroblasts upon the uptake of (A) **1** and (B) **3** in a time window from 1 h to 7 days. Scale bars represent 25 μm. The insets show magnified details of the fiber's elongation and thickening steps.

HOMO−LUMO energy diagram show the expected variations for the change of thiophene to thiophene-*S*-oxide and thiophene-*S*,*S*-dioxide, i.e., a progressively smaller energy gap and higher electron affinity and ionization energy.[14]

The voltammograms in Figure 1B show a quasi-reversible oxidation wave (half-wave potential of 1.10 V) for **1** and an irreversible oxidation wave for the molecules **2** and **3** (half-wave potentials of 1.33 and 1.47 V, respectively) due to the dimerization of the radical cation.[15] The voltammogram of **1** shows two small backward waves, indicating that this trimer was not completely dimerized. No reduction waves are detectable for **1** in the electrochemical stability window of the electrolyte, whereas **2** and **3** show quasi-reversible waves with half-wave potentials at −1.25 and −1.11 V, respectively. If the first oxidation of the trimers enhances the electron affinity more than 0.5 V, it shifts the ionization potential only about 0.2 V. On the other hand, the second oxidation shifts both the electron affinity and the ionization potential 0.22−0.14 V, leading to similar electrochemical band-gaps between the HOMO and LUMO energy levels as confirmed by the maxima of the absorption spectra (Figure 1C).

Then, cell viability, fluorophore uptake, and microfiber production in 2D and 3D cell cultures were deeply evaluated. Compounds **1**−**3** were incubated with 3T3 and B104 cells at a concentration of 50 μg/mL. Figure 2 shows the cell viability assessment through a colorimetric MTT (3-[4,5-dimethylthiazol-2-yl]-2,5-diphenyl tetrazolium bromide) assay that measures the reduction of water-soluble tetrazolium salt by metabolically active cells, thus acting as an indicator of cell viability, proliferation, and cytotoxicity.[16] Both 3T3 cells (Figure 2A) and B104 cells (Figure 2B) treated with compounds **1** and **3** show viability compared to untreated cells (CTR) until 192 h after the treatment. On the contrary, the viabilities of both cell lines incubated with compound **2** drop down to less than 25% that of untreated cells, thus indicating strong cytotoxicity. This result is in accordance with preliminary investigations by LSCM on cells treated with **2** that showed evident alterations in cell morphology, which were probably stress-induced (data not shown). However, deeper investigations into the cytotoxic mechanism exerted by **2** are beyond the main focus of the present study, which is aimed at identifying new thiophene molecules capable of inducing the formation of fluorescent microfibers in live cells. Further dedicated investigations on this point, in comparison with the *S*-oxide of DTTO that showed no toxicity,[11] will be addressed to understand the biochemical mechanisms underlying the cytotoxic effect exerted by compound **2**, with potential applications in fields such as oncology and pharmacology. In

https://doi.org/10.1021/acsomega.1c06677
ACS Omega 2022, 7, 12624−12636

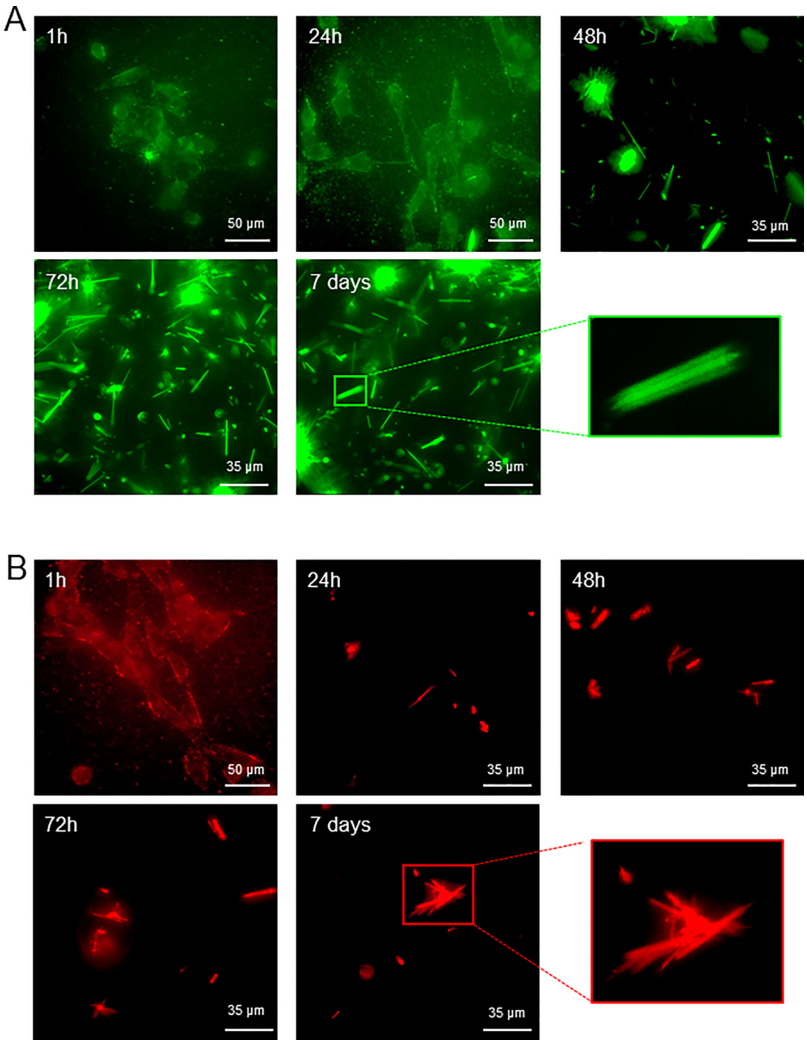

Figure 4. LSCM images of live mouse B104 neuroblastoma cells upon the uptake of (A) **1** and (B) **3** in a time window from 1 h to 7 days. The insets show the lateral assembly of several fibrils or the formation of bundles of microfibers. Scale bars represent 36 μm.

the present framework, it is relevant to point out that MTT assays show that simply modifying the oxygenation of the inner thiophene sulfur (*S*-oxide or *S*,*S*-dioxide) can direct the biological behavior of the resulting terthiophene toward cytotoxic or biocompatible activity. Given the cytotoxic activity of **2**, the monitoring of the biological fate of terthiophenes in 2D and 3D cellular milieu by means of LSCM analyses was limited to fluorophores **1** and **3**.

The cells were incubated for 1 h in serum-free Dulbecco's Modified Eagle Medium (DMEM) containing 50 μg mL^{-1} compound **1** or **3** according to the modalities already described.[8] After, the culture medium was eliminated by repeated washing and replaced with DMEM containing 10% fetal bovine serum (FBS). The cells were cultured for several days and monitored at fixed time intervals by LSCM. All the fluorophores were able to cross the cell membrane and enter the cells (Figures 3 and 4), thus indicating the appropriate hydrophobicity−hydrophilicity balance was able to impart the ability to dissolve into the phospholipidic bilayer and enter the cells; this predominantly occurred by a passive diffusion mechanism. With respect to the result obtained with dithiophene dioxide (DTTO),[8] the uptake of terthiophene dioxide **3** did not lead to the homogeneous diffusion of the fluorophore into the cytoplasm and the following appearance of helical microfibers. Instead, the fluorophore initially accumulated in the perinuclear region, and linear red fluorescent microfibers started to appear on the surface of the cells after 24 h. The density of the fibers increased progressively over time. Then, bundles of fibers appeared, which were likewise assembled via hydrophobic or electrostatic interactions between the corresponding or compatible protein subunits. These results were obtained in both 3T3 cells and B104 cells (Figures 3A and 4A). The same behavior was observed upon treatment with fluorophore **1**, with the appearance of straight green fluorescent microfibers on cell's surface (Figures 3B and 4B).

Some panels of Figure 3 show details that appear as snapshots of various steps of fibers or the formation of bundles of fibers. For example, in Figure 3B the panel relative to seven days after fluorophore uptake indicates that wide fibers are formed layer by layer, while in Figure 4A the panel relative to seven days after fluorophore uptake appears to display the lateral assembly of numerous fibrils; all aggregation processes are favored by the presence of the small fluorophores **1** and **3** (see the photoluminescence of isolated fibers assembled from **1** (Figure S1) and **3** (Figure S2)). Reasonably, the assembly of fibers occurred in the cytoplasm as an intracellular process. This is further shown by the videos (reported as associated

https://doi.org/10.1021/acsomega.1c06677
ACS Omega 2022, 7, 12624−12636

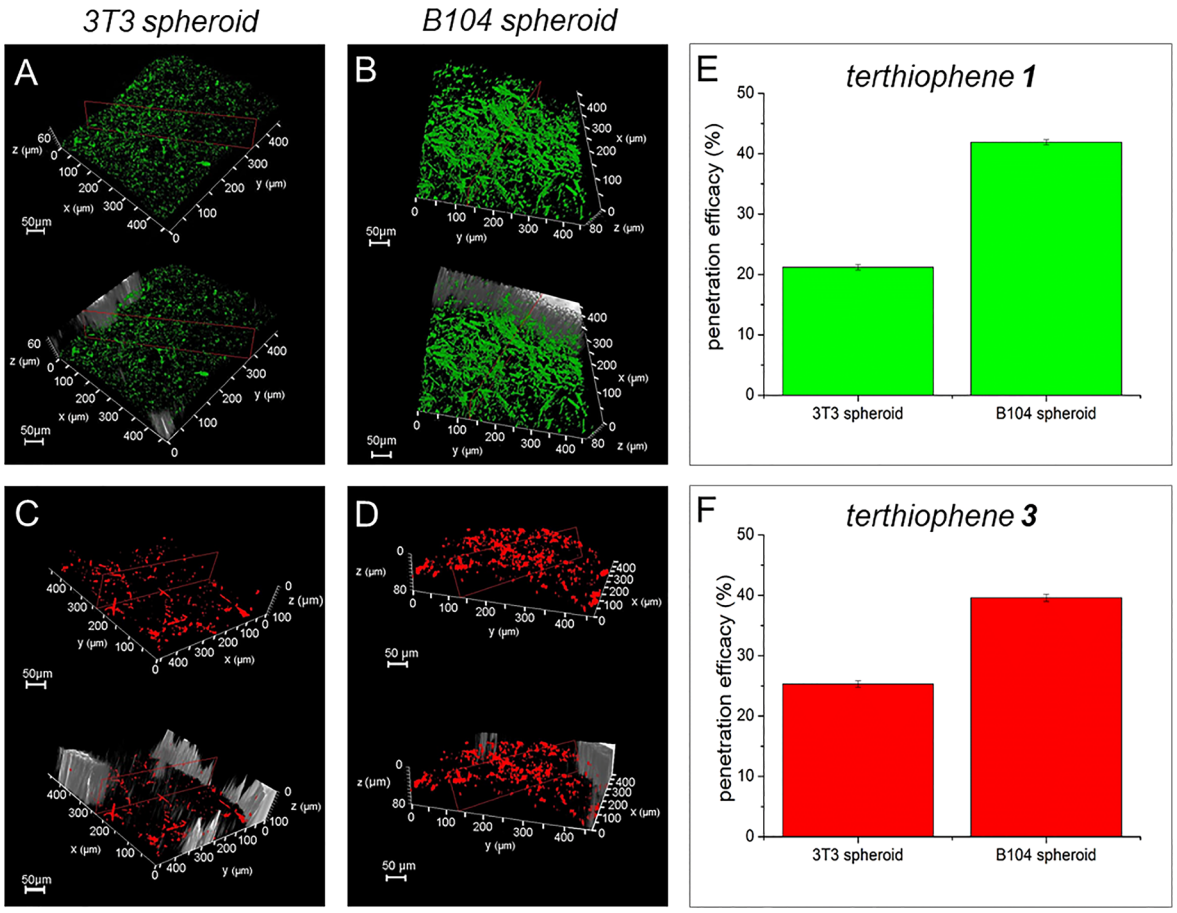

Figure 5. *z*-Stack sections acquired from photoluminescence reconstruction in the *z*-direction of the qualitative fiber production in (A and C) 3D fibroblasts (3T3) and (B and D) neuroblastoma cells (B104) after eight days of incubation with dyes **1** and **3**, respectively. Penetration efficacy analysis of dyes (E) **1** and (F) **3** assessed by fluorescence flow cytometry after eight days in 3D spheroids. Scale bars represent 50 μm. A representative result of three independent experiments is shown.

content) and the *z*-stack sections reported in Figure S3. In particular, the videos reported as associated content show the confocal scanning of the cells along the *z*-axis, demonstrating the subcellular compartmentalization of the fluorescent emission. The different shapes of the intracellularly formed microfibers depends on the proteins the fluorophore is interacting with, as the supramolecular organization of the fluorophore inside the cells is a a protein-templated process. The fluorophores that we describe do not simply label already formed intracellular proteins but instead are recognized and progressively incorporated by the proteins during the fiber formation. For comparison, Figures S4A and S4B show the fluorescence microscopy images of cast films of **1** and **3** on glass in the cell milieu (DMEM) and in toluene, respectively. The comparison allows us to point out that the supramolecular organization of **1** and **3** inside the cells is completely different from that obtained by spontaneous self-assembly in different media, including the culture cell medium DMEM. In addition, we also checked the ability of fluorophores **1** and **3** to penetrate a 3D structure (spheroids of 3T3 and B104 cells) and then promote the production of fibers. A qualitative study performed via confocal microscopy. **1** and **3** demonstrated efficient infiltration into the complex 3D structure of spheroids, thus producing microfibers similar to those obtained with the 2D cell cultures. In addition, quantitative analysis of disaggregated 3D spheroids by fluorescence flow cytometry (Figure 5E and F) confirmed the previous results, thus showing penetration efficacies for both compounds of about 20% in 3T3 spheroids and about 50% for spheroids obtained with B104 neuroblastoma cells. These dissimilar efficacies can be explained by the fact that spheroids obtained by fibroblasts present a complicated and intricate extracellular matrix; however, this limited efficiency of penetration did not preclude the ability of compounds **1** and **3** to induce the formation of fibers.

Further investigations were then directed to assess the chemico-physical properties of isolated fibers. First of all, the fluorescent microfibers identified by LSCM investigations were isolated from the cell lysate seven days after cells were treated with **1** and **3**, and the protein composition was profiled by sodium dodecyl sulfate polyacrylamide gel electrophoresis (SDS-PAGE). Figure 6 shows the resultant stained gel of the isolated fibers produced by 3T3 fibroblasts and B104 neuroblastoma cells after incubation with **1** and **3**. It is clearly evident that the pattern of the proteins is quite the same for all cell lines. In particular, six principal main protein bands were identified in all cased and named from I to VI based on decreasing molecular weight.

Given the similarity of the SDS-PAGE analysis of all the fibers, we chose to characterize more in depth only the fibers directly isolated from 3T3 cells upon incubation with **1** and **3** by means of HPLC-ESI-QTOF analysis and the application of the Mascot software for protein identification (http://www.matrixscience.com/search_intro.html).[17,18] As described in the

https://doi.org/10.1021/acsomega.1c06677
ACS Omega 2022, 7, 12624−12636

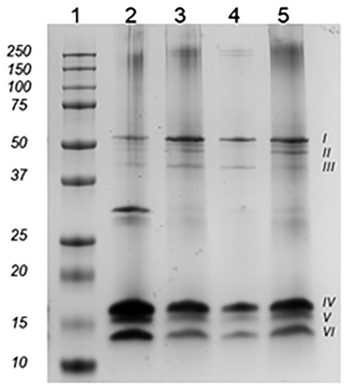

Figure 6. Representative SDS-PAGE of isolated fibers produced by 3T3 fibroblasts (lanes 2 and 3) and B104 neuroblastoma cells (lanes 4 and 5) after incubation with **1** (lanes 2 and 4) and **3** (lanes 3 and 5). Lane 1 shows proteins (markers) of known molecular mass (sizes in kilodaltons are shown on the left). The most representative protein bands identified are named from I to VI (on the right).

Materials and Methods section, the enzymatic cleavage of protein microfibers by trypsin into a mixture of peptides, followed by the separation and identification of peptides by mass spectrometry and the comparison of their molecular weights against an appropriate protein database, afforded lists of identified proteins, which are reported in Tables S1 and S2. It is well-known that establishing the real concentration of a protein in a complex biological system is not a straightforward task.[17,18] Although enzymatic digestion reduces a protein into a much more tractable set of smaller peptides, there are several drawbacks, including the fact that the protein sequence has to be present in the database employed and that the peptides should be present in a single protein and not in a mixture of proteins for the analysis to be correct. To estimate the protein content of our microfibers, we considered the exponentially modified protein abundance index[19] (emPAI, see Tables S1 and S2). The major protein constituents were found to be vimentin (53.6 kDa) and histone H4 (11.4 kDa), which could correspond to bands I and VI, respectively, in Figure 6. Additionally, accessory proteins were recognized with moderate emPAI indices, in particular H2A (13.9 kDa), H2B (14.1 kDa), and H3 (15.3 kDa). These proteins, along with the most abundant protein H4, formed the histone octamer[20] and the globular protein actin (43 kDa) that constituted the microfilaments. The linker histone H1 (22 kDa) was also identified as secondary constituent in the fibers. Moreover, several proteins with lower emPAI indices were listed, thus indicating their accessory role in the fiber's composition with respect to histone H4 and vimentin (see Tables S1 and S2). It was found that fibers from **1** were richer in these accessory proteins than fibers from **3**. In agreement with biochemical data, localization experiments of isolated fluorescent microfibers obtained from 3T3 fibroblasts and B104 neuroblastoma cells after the incubation of dyes **1** and **3** with the fluorescent-labeled monoclonal antivimentin antibody displayed the degree of localization for the antibody in the microfibers. Figure 7 shows images obtained by the LSCM analysis of isolated green (fluorophore **1**, Figure 7A) or red (fluorophore **3**, Figure 7B) fluorescent microfibers with the antivimentin antibody (red or green, respectively) and the corresponding *z*-stack sections.

In particular, *z*-stack reconstruction displays the colocalization of fluorescent microfibers (green for dye **1**, Figure 7A-B)

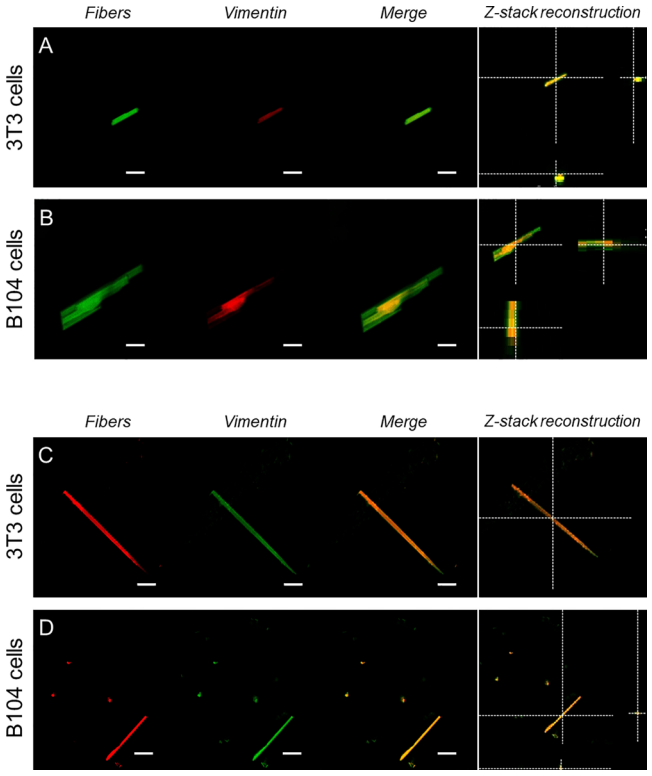

Figure 7. LSCM images of the colocalization experiment between isolated green fluorescent microfibers secreted by (A) 3T3 fibroblasts and (B) B104 mouse neuroblastoma cells treated with **1** and an antivimentin antibody (red). Scale bars represent (A) 10 and (B) 5 μm. Similarly, LSCM images of the colocalization experiment between isolated red fluorescent microfibers secreted by (C) 3T3 fibroblasts and (D) B104 mouse neuroblastoma cells upon treatment with **3** and antivimentin antibody (green). Scale bars represent 10 μm.

or red (dye **3**, Figure 7C–D) with the fluorescence of the antivimentin antibody (red or green, respectively). Videos of colocalization experiments are separately reported as Supporting Information. Vimentin is actively involved in the formation of intermediate filaments (IF) of the cytoskeleton.[21−24] Vimentin IFs are important structures in the perinuclear region that are closely associated with the nucleus, mitochondria, and the endoplasmic reticulum. The multiple interactions of vimentin IFs seem to also be reflected in the microfibers formed upon fluorophore administration. In fact, as mentioned above, all the accessory proteins identified by mass spectrometry analysis in the isolated fibers derived from **1** and **3** suggest a complex network of protein interactions, which supports the idea of fully functional proteins associated in the fibers upon interaction with the small molecules. Interestingly, along with vimentin and histone H4 as main constituents, both **1** and **3** fibers showed the presence of histones H2A, H2B, H3, and H1. This result is supported by SDS-PAGE analysis that showed the presence of low-molecular-weight protein bands (III − VI), presumably associated with histones. These findings again support the hypothesis that the fibers formed upon interaction with the thiophene fluorophores retain the biological activity exerted by vimentin. In fact, this protein is known for its affinity toward nucleic acid, histones, and nuclear matrix proteins.[21−24] The higher prevalence of histone H4 respect to the other constituents of the core histone octamer (H2A, H2B, and H3) that assemble together with DNA as a nucleosome in the nucleus may support the finding that the

https://doi.org/10.1021/acsomega.1c06677
ACS Omega 2022, 7, 12624−12636

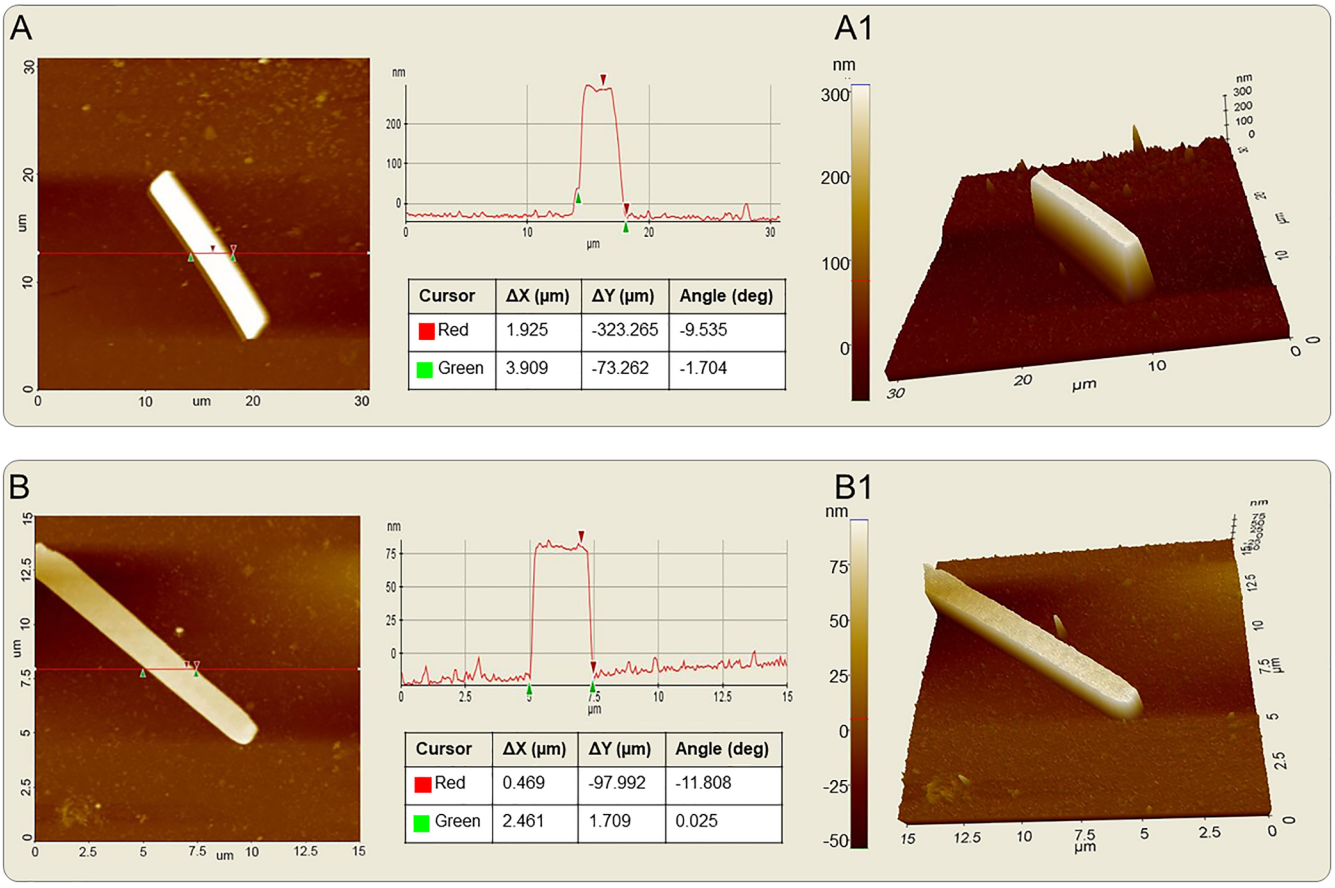

Figure 8. AFM images of isolated microfibers formed by 3T3 fibroblasts upon the uptake of (A) **1** and (B) **3**.Panels A1 and B1 are 3D reconstructions of the corresponding fibers in panels A and B.

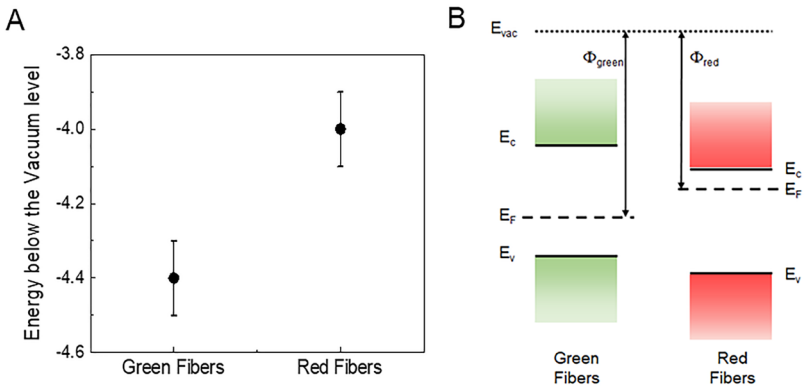

Figure 9. (A and B) Work function values (the difference between the Fermi level and the vacuum energy) of red and green fibers obtained from 3T3 cells upon treatment with **1** or **3** measured by a macroscopic Kelvin probe. Red fibers have a lower work function absolute value (E_F closer to vacuum), which is compatible with an increase of the *n*-type character with respect to green fibers as exemplified in the scheme in panel B.

formation of microfibers between vimentin and histone proteins with terthiophene and its *S*,*S*-dioxide occurred in the cytoplasm. Furthermore, these investigations also show the high affinity of fluorophores **1** and **3** for vimentin and histone H4 when incubated with fibroblasts 3T3, which secrete the collagen protein. This result contracts with the high affinity showed by DTTO for collagen when incubated with 3T3 cells and those for vimentin when incubated with B104 cells. This aspect is of particular relevance for the biomedical implications because vimentin is involved in cancer migration and metastatic progression, thus representing an oncological target of particular relevance.[24] The morphology of the isolated fibers was evaluated by AFM, which showed that the isolated microfibers were chemically stable and their morphology did not change with time. All microfibers are rigidly linear and display very similar morphologies characterized by large aspect ratios several tens of micrometers long, a few micrometers width, and a few tens or hundreds of nanometers thick. As an example, Figure 8 shows the AFM images of the fluorescent microfibers isolated from the cell lysate of 3T3 cells treated with fluorophore **1** (panel A) and **3** (panel B) together with the corresponding 3D reconstruction (panels A1 and B1,

https://doi.org/10.1021/acsomega.1c06677
ACS Omega 2022, 7, 12624−12636

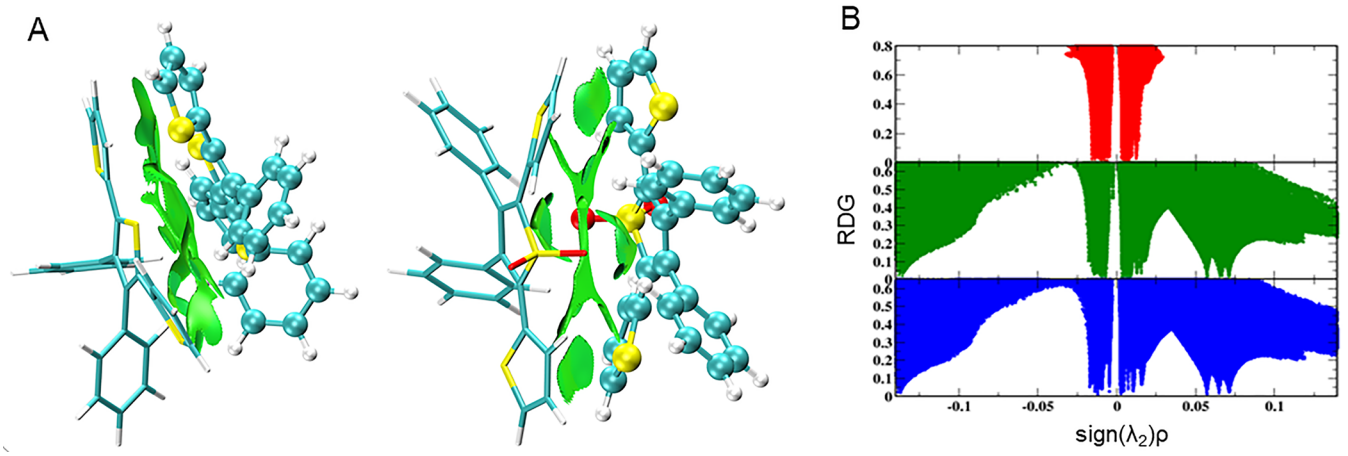

Figure 10. (A) DFT-calculated structures of the dimer of fluorophores **2** (left) and **3** (right). The green region between the two molecules is the noncovalent interaction (NCI) indicator isosurface identifying the nonbonding interaction region between the two molecules. (B) A plot reporting the values of the NCI indicator for the dimers of **1**, **2**, and **3** (from top down). An interaction is present for the reduced density gradient (RDG) tending to zero. If this occurs for small and negative values of sign(λ_2)ρ, the interaction is van der Waals-type. For larger values, the interaction is electrostatic.

respectively). Similarly, the AFM images of the isolated microfibers secreted by B104 cells following treatment with **1** and **3** are shown in Figure S5.

The individual dimensions of the fiber in Figure 8A are length = 20 μm, width = 5 μm, and thickness = 320 nm, while the dimensions of the fiber in Figure 8 B are length = 10 μm, width = 2.5 μm, and thickness = 80 nm. It is worth noting that the morphology of these microfibers is very different from that observed for the isolated microfibers secreted by B104 cells upon treatment with the fluorophore DTTO, which are mainly made of vimentin and display the presence of coiled-coil arrangements.[10] The stiffness observed for the microfibers in Figure 8 most likely arises from the mixture of the composing proteins. Macroscopic Kelvin probe (KP) measurements were carried out on thick drop-casted films of microfibers obtained upon the treatment of 3T3 cells with fluorophores **1** and **3**. The results are shown in Figure 9. KP measures the contact potential difference (CPD) between the sample and a known metal tip from which it is possible to derive the sample work function after the tip is calibrated with a reference material (CPD = $WF_{sample} - WF_{tip}$). This technique has been widely used to characterize the electrical properties of organic supramolecular materials.[25]

Figure 9 shows that the red fibers obtained upon treating the cells with **3** (i.e., the thiophene-*S*,*S*-dioxide derivative) have a work function (absolute) value lower than that of the green fibers obtained upon treating the cells with **1**, i.e., the WF approaches the vacuum level. Analogous to semiconducting materials,[26] this result indicates an increase of the *n*-type character of the red fibers with respect to the green ones. The difference in energy between the two types of microfibers, near 400 mV, is in line with the values for the HOMO and LUMO energies of **1** and **3** that were obtained from cyclovoltammetry (see Figure 1). This finding is a strong indication that the electrical properties of the fibers are directly related to the presence of the embedded fluorophores, whose chemical structures have changed from thiophene (**1**) to thiophene-*S*,*S*-dioxide (**3**). It is well-known that small molecules act as chemical inducers of the interaction between two proteins, leading to the formation of nanofibers with large aspect ratios that in turn promote the lateral assembly into micrometer-scale structures.[5−7] The driving forces are noncovalent interactions, including hydrogen bonding, $\pi-\pi$ stacking, hydrophobic−hydrophilic interactions, and intermolecular interactions between small molecules pertaining to different nanofibrils. In our case we do not know whether vimentin and histone 4, which are the prevalent proteins present in the microfibers, form independent nanofibrils that embed the fluorophore or cofibrils that incorporate the fluorophore and progressively grow by the parallel association of a large number of fibrils. Nevertheless, the ability of small molecules to induce protein association implies that intermolecular interactions between a fluorophore belonging to a filament and another fluorophore belonging to a different filament must play a role in both cases. With this in mind, we used DFT calculations (http://www.turbomole.com)[27−29] to analyze the aggregation modalities of fluorophores **1** and **3** to gain clues about possible changes to introduce to their structures for better performance. For the sake of completeness, we have also extended this study to *S*-oxide **2** (see Figure S6). Figure 10 shows the preferred configurations of the dimers of **1** and **3** and the noncovalent interaction (NCI) indicator isosurface (the green region between the two molecules) identifying the nonbonding interactions between the two molecules.

The optimal structures of the dimers were identified by performing a preliminary screening of a large number of structures (about 250 per molecule) generated by random displacements of the monomers. Subsequently, the 50 best candidates were optimized, and the most stable configurations were identified. The dominant interactions in all fluorophores are the $\pi-\pi$ stacking type. In **1**, they are the only interactions present. Fluorophores **2** and **3**, owing to the presence of sulfur−oxygen bonds (Figure 10A), have a dipole, giving rise to dipole−dipole interactions and hence to a contribution from the electrostatic effect. The interaction energies and the average distances between the two molecules of **1** are 1.058 eV and 5.5 Å, those of **2** are 1.346 eV and 4.8 Å, and the corresponding ones for **3** are 1.185 eV and 4.9 Å. For the dimer of **1**, the relative orientation of the two molecules does not appreciably change the interaction energy due to the lack of a dipole moment. In contract, there are preferred orientations for the dimers of **2** and **3**. In **2**, the sulfur atoms

https://doi.org/10.1021/acsomega.1c06677
ACS Omega 2022, 7, 12624−12636

of the thiophene rings point in opposite directions, while those in **3** are located about 90° apart. In **2**, the dipoles point in opposite directions. In **3**, however, there are two factors opposing this possibility. On one side, owing to the greater polarization due to the presence of two sulfur−oxygen bonds, the phenyl groups are more positive and are consequently pushed apart from each other. On the other side, the oxygen atoms are outside the molecular plane and generate a steric interaction with the p orbitals of the adjacent molecule. In consequence, the final configuration is a compromise between dipole−dipole attraction and steric repulsion. This causes the interaction energy in the dimer of **3** to be smaller than that in the dimer of **2**. Figure 10B shows the DFT-calculated structures of the dimers of fluorophores **2** (left, two *S*-oxides)) and **3** (right, two *S*,*S*-dioxides). The region in green between the two molecules is the plot of the NCI surface where the interaction is localized. Figure 10B shows the plot of NCI values, which indicate the nature of the interactions present. An interaction is present for a reduced density gradient (RDG) tending to zero. If sign(λ_2)ρ is small and negative, the interaction is the van der Waals type, while for larger values the interaction is electrostatic (dipole−dipole or H-bonding). On the basis of experimental and theoretical data and by analogy with the formation of type I collagen and DTTO fibers, we can summarize the process of terthiophene fiber formation as follows. Having the appropriate hydrophobicity−hydrophilicity balance, compounds **1**−**3** are able to cross the cell membrane and enter the cells in both 2D and 3D cell cultures. Our experimental evidence suggests a common underlying mechanism for the assembly of protein−DTTO[8−11] and protein−terthiophene nano- or microfibers, which at least for now are the only examples of fiber formation in live cells upon treatment with small thiophene-based fluorophores. The secretion of the fibers is promoted by cell's machinery, and their formation—through small molecule-assisted assembly mechanism, which is probably a common occurrence in living cells—is traceable thanks to the fluorescence properties of the small-molecular fluorophores. The pathway for fiber formation starts in the cytoplasm and includes a nucleation process with the formation of various oligomers, followed by a lag phase and subsequent lateral growth and layer-by-layer thickening according to kinetics that depend on experimental conditions (concentration, temperature, etc.). A fiber's size and density increase progressively overtime. Once the fiber's size has reached a given (so far unknown) range, it is moved to the surface of the cells.

Finally, we highlight that the microfibers described in this work are peculiarly different from protein microfibers prepared by in vitro self-assembly methods that allow rational peptide and protein design.[1] In these cases, the specific properties of the fibers depend largely on the fabrication method, but property standardization has not yet been done. In our case, the assembly process takes place in vivo and is regulated by the cell's own machinery.[8−10] At the present stage of knowledge, our microfibers are difficult to control in structure, exact composition, size distribution, etc. This is why we believe that a direct comparison with the characteristics reported for the numerous protein microfibers described so far would be unrealistic. As also briefly mentioned in the introduction, initial results show that these microfibers have potential for tissue engineering and conferring bioactivity to synthetic scaffolds once they are isolated by the cell lysate.[10] Moreover, as demonstrated in this work for the first time, potential *p*- or *n*-type charge conduction properties can be imparted to the microfibers spontaneously formed inside the cells by choosing the appropriate thiophene fluorophore. Thus, one can also speculate that guided, controlled, and noninvasive ways to measure the in situ conduction of the microfibers could be implemented using nanotechnology methods. This would pave the way to the realization of electronics built into the cells by their own machinery, allowing for remote tracking and the control of both cell behavior and microfiber formation. Last but not least, the formation of fluorescent fibers will allow in situ studies in real time on the dynamics of proteins assembly.

CONCLUSIONS

We have described the behavior of a set of fluorescent terthiophenes inside live 3T3 fibroblasts and B104 neuroblastoma cells and demonstrated that the biological fate of the cells can be directed toward cytotoxic or biocompatible activity by simply oxygenating the inner thiophene sulfur of unmodified terthiophene **1** to the corresponding *S*-oxide (**2**) or *S*,*S*-dioxide (**3**). Indeed, a cell viability assessment through a colorimetric MTT test following the incubation of **1**−**3** with 3T3 and B104 cells shows that the viabilities of both cell lines incubated with compound **2** drop to less than 25% that of untreated cells, thus indicating strong cytotoxicity. By contrast, both cell lines treated with compounds **1** and **3** show viabilities comparable to that of untreated cells. Moreover, terthiophenes **1** and **3** are capable of inducing the in situ aggregation of specific proteins into micrometer-sized fibers displaying fluorescent and electroactivity properties. Spontaneous formation of microfibers was observed in both 2D and 3D cell cultures, the latter of which were observed for the first time. Compared to the microfibers obtained after treating the cells with unmodified terthiophene **1**, the optical and electrical properties of those obtained following treatment with *S*,*S*-dioxide **3** result in the red-shifted fluorescence, increased electron affinity, and increased *n*-type characteristic of the microfibers. The changes are in line with what has already been observed for thiophene-*S*,*S*-dioxide-containing materials with respect to those containing the corresponding thiophene counterpart.[11] Thus, the changes in optical and electrical properties of the microfibers spontaneously formed inside live cells are predictable on the basis of the molecular structural changes introduced in the fluorophore employed. In this way, a chemical input is transformed into a modification of the optical and electrical properties of protein microfibers. Additionally, our results reveal the high affinity of fluorophores **1** and **3** for vimentin and histone H4, which are prevalent proteins that compose the microfibers formed inside the cells, as shown by Q-TOF mass spectrometry analysis. Vimentin is actively involved in the formation of IFs of the cytoskeleton,[21−23] which are important structures in the perinuclear region that are closely associated with the nucleus, mitochondria, and the endoplasmic reticulum. The multiple interactions of vimentin IFs seem to also be reflected in the microfibers formed upon fluorophore administration. In fact, all the accessory proteins identified by mass spectrometry analysis of the isolated fibers derived from **1** and **3** suggest a complex network of protein interactions, supporting the idea that the fibers formed upon interaction with the thiophene fluorophores retain the biological activity exerted by their protein constituents. These results add interesting perspectives to the use of a specific chemical input, i.e., terthiophene fluorophores, to direct the coassembly of novel biomaterials with a specific

https://doi.org/10.1021/acsomega.1c06677
ACS Omega 2022, 7, 12624−12636

protein composition. In fact, once isolated from the cells, microfibers such as those described here could find applications as biomaterials in various medical and technological applications (from drug delivery to tissue engineering, protein-based diagnostic sensors, etc.). Our data also show that theoretical calculations could help optimize the molecular structure and the intermolecular interactions between the small molecules inducing microfiber formation inside live cells. More importantly, they could furnish information about the way the molecules should be organized to create a supramolecular pattern capable to favoring charge mobility. In a longer perspective, this could open the door to the realization of electronics built inside the cells by their own machinery.

EXPERIMENTAL SECTION

Materials. All tissue culture media and chemical reagents were purchased from Sigma-Aldrich. Cell lines were purchased from the American Tissue Type Collection (ATTC).

Cyclic Voltammetry. Cyclic voltammograms (CVs) were recorded at 100 mV s^{-1} in 0.2 mmol L^{-1} $(C_4H_9)_4NClO_4$ (Fluka electrochemical-grade, dried under reduced pressure) in CH_2Cl_2 (distilled on P_2O_5 and stored under Ar pressure), where the potential of the aqueous satured calomel electrode (SCE) was −0.475 V vs ferrocene/ferricenium. **1**−**3** were separately tested at the concentration of 1 mmol L^{-1} in a three-compartment glass cell using an AMEL 5000 electrochemical system. The working electrode was Pt, the reference electrode was SCE, and the auxiliary electrode was Pg wire.[2]

Cell Cultures in 2D and 3D. Mouse embryonic fibroblasts (3T3) and mouse neuroblastoma (B104) were maintained in DMEM supplemented with 10% FBS, 100 U mL^{-1} penicillin, 100 mg mL^{-1} streptomycin, 5% L-glutamine, and 5% sodium pyruvate in a humidified incubator at 37 °C, 5% CO_2, and 95% relative humidity. For adherent 2D cultures of 3T3 and B104 cells, an appropriate number of cells (10^5 cells) were incubated for 1 h in the serum-free DMEM culture medium containing the different fluorophores at a concentration of 50 μg mL^{-1}, according to the modalities described in ref 8. Afterward, the culture medium was eliminated by repeated washing and entirely replaced with DMEM supplemented with 10% FBS. Then, the cells were cultured for several days and monitored at fixed time intervals by LSCM using a Leica confocal scanning system mounted onto a Leica TCS SP5 (Leica Microsystem GmbH, Mannheim, Germany) instrument. Spheroids derived from 3T3 and B104 cells (3D cultures) were produced by seeding cells (10^4 cells) on 1.5% agarose-coated 96-well plates. After three days, only uniform and compact spheroids were treated with the dyes at a concentration of 50 μg mL^{-1}. After eight days of incubation, spheroids were fixed with 4% paraformaldehyde for 10 min and then analyzed on a confocal Leica TCS SP8 (Leica Microsystem GmbH, Mannheim, Germany) system for the qualitative analysis of the dye's penetration and fiber production capability. For quantitative analysis, after eight days of incubations with the dyes, the spheroids were disaggregated with 0.25% trypsin plus pipetting, centrifugated, fixed with 4% paraformaldehyde for 10 min, and analyzed with a flow cytometer (Accuri C6, BD, USA) by counting 10 000 ungated cells.

Cell Viability Assay. 3T3 and B104 cells (10^5 cells) were incubated for 1 h in DMEM without FBS containing the different fluorophores at a concentration of 50 μg mL^{-1} for a time window up to 192 h. Untreated (CTR) samples were used as the control groups. Cell viability was evaluated by the MTT assay (Sigma-Aldrich) according to the manufacturer's instructions. Briefly, after a proper incubation time, the MTT solution was added to cultures. The mixture was incubated in an incubator for 3 h, and the resulting MTT formazan crystals were dissolved with an acidified isopropanol solution. The absorbance was spectrophotometrically measured at a wavelength of 570 nm. The cell viability is expressed as the relative growth rate (%, RGR) by the following equation: $RGR = \frac{D_{sample}}{D_{control}} \times 100$where D_{sample} and $D_{control}$ were the absorbances of the sample and the negative control, respectively.

Isolation of Fluorescent Fibers. The isolation of fluorescent fibers was performed as previously described.[8,10] Briefly, cells treated with fluorescent dyes as describe above were gently scraped off the bottom of the flask into the medium after eight days. In the resulting cell suspension, fluorescent fibers were isolated by cells using a lysis solution (50 mM Tris HCl, pH 7.4; 1% Triton X-100; 5 mM EDTA; 150 mM NaCl, 1 mM Na_3VO_4; 1 mM NaF; 1 mM phenylmethylsulfonyl fluoride (PMSF); and protease inhibitor cocktail) and incubated at 4 °C. Fluorescent fibers were left to decant, harvested into fresh reaction tubes, washed three times with fresh lysis buffer by centrifugation, and stored at 4 °C or −80 °C until characterization analyses were performed.

SDS-PAGE. Dilution samples of dye fibers isolated from cells were separated on SDS-PAGE gels (gradient of 4−15%, Mini-PROTEAN TGX precast protein gels) without prior heating. Resolved protein bands were visualized by Coomassie staining (Sigma Chemical Co., St. Louis, MO) according to the manufacturer's instructions. Resolved bands were analyzed using ChemiDoc MP instruments (Biorad).

Tryptic Digestion and Mass Spectrometry Analysis. Fibers isolated from mouse embryonic fibroblasts (3T3) were resuspended with 8 M urea and treated with 5 μL of 100 mM ammonium bicarbonate (AMBIC), reduced with 10 mM dithiothreitol (DTT, 1 μL in 100 mM AMBIC) at 56 °C for 30 min, and alkylated with55 mM iodoacetamide (1 μL in 100 mM AMBIC) at room temperature in the dark for 1 h. The resulting protein mixture was digested with TPCK-modified sequencing-grade trypsin (the final ratio of enzyme to substrate was 1:50 w/w) at 37 °C overnight. Samples were then acidified with 1 μL of a 5% formic acid (FA) solution and dried in a vacuum evaporator. Trypsinized microfibers were resuspended in 40 μL of water/acetonitrile/formic acid (95:3:2), sonicated, and centrifuged, then 35 μL of this solution was injected into a UHPLC system (Ultimate 3000, Dionex, Thermo-Fisher Scientific) coupled to a Q Exactive mass spectrometer (Thermo-Fisher Scientific) equipped with a HESI-II ion source. Peptides were loaded into a C18 Hypersil Gold (100 × 2.1 mm ID, 1.9 μm ps) column (Thermo-Fisher Scientific) and separated using a linear gradient of 0.1% formic acid in water (A) and acetonitrile (B) from 2% B to 28% B in 90 min. The mass spectrometer was operated with a data-dependent acquisition (DDA) method by performing a $250 < m/z < 2000$ full MS scan at 70 000 resolution (at m/z 200), followed by HCD fragmentation at 28 normalized collision energies of the six most intense precursor ions (charge state $z \geq 2$ 17 500 resolution (at m/z 200), with a dynamic exclusion of 10 s. Raw data files were converted to the mascot generic format (.mgf) using MSConvert (http://www.proteowizard.org/tools/msconvert.html), and protein identification was performed using Mascot Server (ver. 2.7.0) search engine against the

https://doi.org/10.1021/acsomega.1c06677
ACS Omega 2022, 7, 12624−12636

Swissprot database (release 2018_05) and a database of contaminants commonly found in proteomics experiments (cRAP). The search parameters were set as follows: trypsin was selected as enzyme with one missed cleavage allowed; carbamidomethylation (C) was specified as fixed modification; oxidation (M) and deamidation (NQ) were specified as variable modifications; and peptide and MS/MS tolerances were 10 ppm (#^{13}C = 1) and 0.02 Da, respectively. A false discovery rate (FDR) evaluation was performed using a decoy concatenated search, and results were filtered at 1% FDR for peptide spectrum matches (PSMs) above homology, narrowing the search to the *Mus musculus* proteome.

Atomic Force Microscopy (AFM). The isolated microfibers were deposited by drop-casting on silicon substrates. Noncontact AFM (NC-AFM) imaging of isolated fluorescent fibers was performed with a XE-100 Park Systems AFM equipped with large -area scanners (100 μm × 100 μm).

Kelvin Probe Characterizations. Kelvin probe measurements were performed using a 2 mm diameter gold tip (ambient Kelvin probe package from KP Technology Ltd.) Probe calibration was performed versus freshly cleaved and highly oriented pyrolytic graphite as the reference surface. The measurements were done on thick films of fibers obtained by drop-casting.

DFT Calculations. All DFT calculations were performed using the TURBOMOLE program package (http://www.turbomole.com)[27−33] and the multipole accelerated resolution of identity approximation.[28] The preliminary screening of the dimers structures was carried out at the PBE0-D3/def2-SV(P) level of theory.[29,33] The final optimization of the structures and the investigation of isolated molecules was performed at the PBE0-D3/def2-TZVP level of theory.[29,33]

■ ASSOCIATED CONTENT

Supporting Information

The Supporting Information is available free of charge at https://pubs.acs.org/doi/10.1021/acsomega.1c06677.

Synthesis of compounds **1**−**3**, optical cahracterizations of fibers, LSCM *z*-stack sections of 3T3 and B104 cells, fluorescence microscopy images, mass spectrometry-based protein identification of isolated fibers **1** and **3**, ARM images of isolated microfibers, and DFT calculations of **2** (PDF)

LSCM video of 3T3 cells with fibers obtained by **1** (MP4)

LSCM video of 3T3 cells with fibers obtained by **3** (MP4)

LSCM video of B104 cells with fibers obtained by **1** (MP4)

LSCM video of B104 cells with fibers obtained by **3** (MP4)

LSCM video of the colocalization between compound **1** and vimentin in microfibers produced in 3T3 cells (MP4)

LSCM video of the colocalization between compound **1** and vimentin in microfibers produced in B104 cells (MP4)

LSCM video of the colocalization between compound **3** and vimentin in microfibers produced in B104 cells (MP4)

LSCM video of the colocalization between compound **3** and vimentin in microfibers produced in 3T3 cells (MP4)

■ AUTHOR INFORMATION

Corresponding Author

Ilaria Elena Palamà − *Nanotechnology Institute (CNR-NANOTEC), University of Salento, 73100 Lecce, Italy;* orcid.org/0000-0003-4420-0680; Email: ilaria.palama@nanotec.cnr.it

Authors

Gabriele Maiorano − *Nanotechnology Institute (CNR-NANOTEC), University of Salento, 73100 Lecce, Italy*

Francesca Di Maria − *CNR-ISOF and Mediteknology srl Area Ricerca CNR, 40129 Bologna, Italy;* orcid.org/0000-0001-5557-3816

Mattia Zangoli − *CNR-ISOF and Mediteknology srl Area Ricerca CNR, 40129 Bologna, Italy;* orcid.org/0000-0002-0340-9245

Andrea Candini − *CNR-ISOF and Mediteknology srl Area Ricerca CNR, 40129 Bologna, Italy;* orcid.org/0000-0003-3909-473X

Alberto Zanelli − *CNR-ISOF and Mediteknology srl Area Ricerca CNR, 40129 Bologna, Italy*

Stefania D'Amone − *Nanotechnology Institute (CNR-NANOTEC), University of Salento, 73100 Lecce, Italy*

Eduardo Fabiano − *Institute for Microelectronics and Microsystems (CNR-IMM), 73100 Lecce, Italy; Center for Biomolecular Nanotechnologies, UNILE Istituto Italiano di Tecnologia, 73010 Arnesano, Italy*

Giuseppe Gigli − *Nanotechnology Institute (CNR-NANOTEC) and Department of Mathematics and Physics, University of Salento, 73100 Lecce, Italy*

Giovanna Barbarella − *CNR-ISOF and Mediteknology srl Area Ricerca CNR, 40129 Bologna, Italy*

Complete contact information is available at: https://pubs.acs.org/10.1021/acsomega.1c06677

Author Contributions

[§]These authors contributed equally.

Notes

The authors declare no competing financial interest.

■ ACKNOWLEDGMENTS

This study was supported by "Tecnopolo di Nanotecnologia e Fotonica per la medicina di precisione" (TECNOMED) (FISR/MIUR-CNR delibera CIPE no. 3449 del 7-08-2017, CUP B83B17000010001), "Tecnopolo per la medicina di precisione" (TecnoMed Puglia) (Regione Puglia DGR no. 2117 del 21/11/2018, CUP B84I18000540002), and the Progetto PON ARS01_00906 "TITAN - Nanotecnologie per l'immunoterapia dei tumori" (supported by FESR PON "Ricerca e Innovazione" 2014−2020-Azione II-OS 1.b). F.D.M, G.B., and M.Z. acknowledge financial support from the UE project INFUSION (proposal no. 734834 "Engineering optoelectronic INterfaces: A global action intersecting FUndamental conceptS and technology implementatION of self-organized organic materials"). Finally, the authors acknowledge the "Fondazione Cassa di Risparmio di Modena" for funding the UHPLC-ESI-Q Exactive system at the Centro

https://doi.org/10.1021/acsomega.1c06677
ACS Omega 2022, 7, 12624−12636

Interdipartimentale Grandi Strumenti (CIGS) of the University of Modena and Reggio Emilia.

REFERENCES

(1) DeFrates, K. G.; Moore, R.; Borgesi, J.; Lin, G.; Mulderig, T.; Beachley, V.; Hu, X. Protein-Based Fiber Materials in Medicine: A Review. *Nanomaterials* **2018**, *8* (7), 457. From NLM.

(2) Wang, M.-D.; Huang, Y.-Q.; Wang, H. In Vivo Self-Assembly of Polypeptide-Based Nanomaterials. In *Handbook of Macrocyclic Supramolecular Assembly*; Liu, Y., Chen, Y., Zhang, H.-Y., Eds.; Springer Singapore, 2019; pp 1023−1043.

(3) Schreiber, S. L. Chemical genetics resulting from a passion for synthetic organic chemistry. *Bioorg. Med. Chem.* **1998**, *6* (8), 1127−1152. From NLM. Schreiber, S. L. A Chemical Biology View of Bioactive Small Molecules and a Binder-Based Approach to Connect Biology to Precision Medicines. *Isr. J. Chem.* **2019**, *59* (1−2), 52−59.

(4) Cheng, P. N.; Liu, C.; Zhao, M.; Eisenberg, D.; Nowick, J. S. Amyloid β-sheet mimics that antagonize protein aggregation and reduce amyloid toxicity. *Nat. Chem.* **2012**, *4* (11), 927−933. From NLM.

(5) Hume, J.; Sun, J.; Jacquet, R.; Renfrew, P. D.; Martin, J. A.; Bonneau, R.; Gilchrist, M. L.; Montclare, J. K. Engineered Coiled-Coil Protein Microfibers. *Biomacromolecules* **2014**, *15* (10), 3503−3510.

(6) McFedries, A.; Schwaid, A.; Saghatelian, A. Methods for the elucidation of protein-small molecule interactions. *Chem. Biol.* **2013**, *20* (5), 667−673. From NLM

(7) Nishad Fathima, N.; Saranya Devi, R.; Rekha, K. B.; Dhathathreyan, A. Collagen-curcumin interaction — A physicochemical study. *Journal of Chemical Sciences* **2009**, *121* (4), 509−514.

(8) Palamà, I.; Di Maria, F.; Viola, I.; Fabiano, E.; Gigli, G.; Bettini, C.; Barbarella, G. Live-Cell-Permeant Thiophene Fluorophores and Cell-Mediated Formation of Fluorescent Fibrils. *J. Am. Chem. Soc.* **2011**, *133* (44), 17777−17785.

(9) Moros, M.; Di Maria, F.; Dardano, P.; Tommasini, G.; Castillo-Michel, H.; Kovtun, A.; Zangoli, M.; Blasio, M.; De Stefano, L.; Tino, A.; et al. In Vivo Bioengineering of Fluorescent Conductive Protein-Dye Microfibers. *iScience* **2020**, *23* (4), 101022.

(10) Palamà, I. E.; Di Maria, F.; D'Amone, S.; Barbarella, G.; Gigli, G. Biocompatible and biodegradable fluorescent microfibers physiologically secreted by live cells upon spontaneous uptake of thiophene fluorophore. *J. Mater. Chem. B* **2015**, *3* (1), 151−158.

(11) Di Maria, F.; Zangoli, M.; Palamá, I. E.; Fabiano, E.; Zanelli, A.; Monari, M.; Perinot, A.; Caironi, M.; Maiorano, V.; Maggiore, A.; et al. Improving the Property-Function Tuning Range of Thiophene Materials via Facile Synthesis of Oligo/Polythiophene-S-Oxides and Mixed Oligo/Polythiophene-S-Oxides/Oligo/Polythiophene-S,S-Dioxides. *Adv. Funct. Mater.* **2016**, *26* (38), 6970−6984.

(12) Dell, E. J.; Capozzi, B.; Xia, J.; Venkataraman, L.; Campos, L. M. Molecular length dictates the nature of charge carriers in single-molecule junctions of oxidized oligothiophenes. *Nat. Chem.* **2015**, *7* (3), 209−214.

(13) Barbarella, G.; Zangoli, M.; Di Maria, F. Chapter Three - Synthesis and Applications of Thiophene Derivatives as Organic Materials. In *Advances in Heterocyclic Chemistry.*, Vol. *123*; Scriven, E. F. V., Ramsden, C. A., Eds.; Academic Press, 2017; pp 105−167.

(14) Barbarella, G.; Favaretto, L.; Zambianchi, M.; Pudova, O.; Arbizzani, C.; Bongini, A.; Mastragostino, M. From Easily Oxidized to Easily Reduced Thiophene-Based Materials. *Adv. Mater.* **1998**, *10* (7), 551−554. Wei, S.; Xia, J.; Dell, E. J.; Jiang, Y.; Song, R.; Lee, H.; Rodenbough, P.; Briseno, A. L.; Campos, L. M. Bandgap Engineering through Controlled Oxidation of Polythiophenes. *Angew. Chem., Int. Ed.* **2014**, *53* (7), 1832−1836.

(15) Arbizzani, C.; Bongini, A.; Mastragostino, M.; Zanelli, A.; Barbarella, G.; Zambianchi, M. Polyalkylthiophenes as electrochromic materials: A comparative study of poly(3-methylthiophenes) and poly(3-hexylthiophenes). *Adv. Mater.* **1995**, *7* (6), 571−574.

(16) van Meerloo, J.; Kaspers, G. J.; Cloos, J. Cell sensitivity assays: the MTT assay. *Methods Mol. Biol.* **2011**, *731*, 237−245. From NLM.

(17) Perkins, D. N.; Pappin, D. J.; Creasy, D. M.; Cottrell, J. S. Probability-based protein identification by searching sequence databases using mass spectrometry data. *Electrophoresis* **1999**, *20* (18), 3551−3567.

(18) van de Merbel, N. C Protein quantification by LC-MS: A decade of progress through the pages of Bioanalysis. *Bioanalysis* **2019**, *11* (7), 629−644.

(19) Ishihama, Y.; Oda, Y.; Tabata, T.; Sato, T.; Nagasu, T.; Rappsilber, J.; Mann, M. Exponentially modified protein abundance index (emPAI) for estimation of absolute protein amount in proteomics by the number of sequenced peptides per protein. *Mol. Cell Proteomics* **2005**, *4* (9), 1265−1272. From NLM. Shinoda, K.; Tomita, M.; Ishihama, Y. emPAI Calc—for the estimation of protein abundance from large-scale identification data by liquid chromatography-tandem mass spectrometry. *Bioinformatics* **2010**, *26* (4), 576−577.

(20) Bilokapic, S.; Strauss, M.; Halic, M. Structural rearrangements of the histone octamer translocate DNA. *Nat. Commun.* **2018**, *9* (1), 1330.

(21) Katsumoto, T.; Mitsushima, A.; Kurimura, T. The role of the vimentin intermediate filaments in rat 3Y1 cells elucidated by immunoelectron microscopy and computer-graphic reconstruction. *Biol. Cell* **1990**, *68* (2), 139−146. From NLM.

(22) Danielsson, F.; Peterson, M. K.; Caldeira Araújo, H.; Lautenschläger, F.; Gad, A. K. B. Vimentin Diversity in Health and Disease. *Cells* **2018**, *7* (10), 147.

(23) Sliogeryte, K.; Gavara, N. Vimentin Plays a Crucial Role in Fibroblast Ageing by Regulating Biophysical Properties and Cell Migration. *Cells* **2019**, *8* (10), 1164. From NLM.

(24) Strouhalova, K.; Přechová, M.; Gandalovičová, A.; Brábek, J.; Gregor, M.; Rosel, D. Vimentin Intermediate Filaments as Potential Target for Cancer Treatment. *Cancers (Basel)* **2020**, *12* (1), 184. From NLM.

(25) Liscio, A.; Palermo, V.; Samorì, P. Nanoscale Quantitative Measurement of the Potential of Charged Nanostructures by Electrostatic and Kelvin Probe Force Microscopy: Unraveling Electronic Processes in Complex Materials. *Acc. Chem. Res.* **2010**, *43* (4), 541−550. Melitz, W.; Shen, J.; Kummel, A. C.; Lee, S. Kelvin probe force microscopy and its application. *Surf. Sci. Rep.* **2011**, *66* (1), 1−27.

(26) Di Maria, F.; Zangoli, M.; Gazzano, M.; Fabiano, E.; Gentili, D.; Zanelli, A.; Fermi, A.; Bergamini, G.; Bonifazi, D.; Perinot, A.; et al. Controlling the Functional Properties of Oligothiophene Crystalline Nano/Microfibers via Tailoring of the Self-Assembling Molecular Precursors. *Adv. Funct. Mater.* **2018**, *28* (32), 1801946.

(27) Furche, F.; Ahlrichs, R.; Hättig, C.; Klopper, W.; Sierka, M.; Weigend, F. Turbomole. *WIREs Computational Molecular Science* **2014**, *4* (2), 91−100.

(28) Sierka, M.; Hogekamp, A.; Ahlrichs, R. Fast evaluation of the Coulomb potential for electron densities using multipole accelerated resolution of identity approximation. *J. Chem. Phys.* **2003**, *118* (20), 9136−9148.

(29) Perdew, J. P.; Ernzerhof, M.; Burke, K. Rationale for mixing exact exchange with density functional approximations. *J. Chem. Phys.* **1996**, *105* (22), 9982−9985.

(30) Ernzerhof, M.; Scuseria, G. E. Assessment of the Perdew-Burke-Ernzerhof exchange-correlation functional. *J. Chem. Phys.* **1999**, *110* (11), 5029−5036.

(31) Grimme, S.; Antony, J.; Ehrlich, S.; Krieg, H. A consistent and accurate ab initio parametrization of density functional dispersion correction (DFT-D) for the 94 elements H-Pu. *J. Chem. Phys.* **2010**, *132* (15), 154104.

(32) Rappoport, D.; Furche, F. Property-optimized Gaussian basis sets for molecular response calculations. *J. Chem. Phys.* **2010**, *133* (13), 134105.

(33) Adamo, C.; Barone, V. Toward reliable density functional methods without adjustable parameters: The PBE0 model. *J. Chem. Phys.* **1999**, *110* (13), 6158−6170.

https://doi.org/10.1021/acsomega.1c06677
ACS Omega 2022, 7, 12624−12636